

Thermal Characterisation of Rectangular Cooling Shapes in Heat Generating Mediums – A Three-Dimensional Investigation

Jaco Dirker¹, Arnaud G. Malan², and Josua .P. Meyer^{2*}

¹*Department of Mechanical Engineering, Rand Afrikaans University, Johannesburg, South Africa*

²*Department of Mechanical and Aeronautical Engineering, University of Pretoria, Pretoria, South Africa,*

* *jmeyer@up.ac.za*

Abstract

The optimum aspect ratios of uniformly distributed embedded rectangular cross-sectioned solid cooling inserts in a heat-generating medium are investigated. Numerical investigations were performed to determine and characterise how various geometric and thermal parameters determine these optimum shapes.

Introduction

The current trend in power electronics is to increase the power conversion capability of circuits while reducing their size. One such a way is by means of three-dimensional integration of discrete components into multifunctional modules and the creation of standardized building blocks [1]. This can be done by using planar type structures or modules with various layers [2].

In order to satisfy future thermal demands associated with, for instance, integrated power electronic devices, the focus is starting to shift toward innovative design of the internal structure of power modules to assist in heat extraction, while maintaining high levels of electromagnetic performance and efficiency.

Such an integrated power electronics system requires advances in different technologies, which depend upon finding solutions to deal with the multi-disciplinary issues in materials, electromagnetic compatibility and thermal management.

Purpose

Due to the manufacturing method proposed for constructing the new type of integrated power electronic modules, the cooling inserts would need to have rectangular cross-sections. It is the aim of this paper to describe the optimum aspect ratio of the cooling insert's cross section such that the peak temperature within the heat-generating medium would be minimised. Little reference material was found in literature that describes the optimisation of such geometries. By characterising the influence of various parameters on the optimum cooling structure shape, the design of such embedded cooling systems are enabled.

Procedure

A numerical approach was followed in the study, as it would have been too time-consuming and costly to do the optimisation processes experimentally.

Consider Fig. 1 that gives a representation of a proposed method of assisting heat flow from within a heat-generating medium to the surroundings. The sectioned view shows a generalised distribution of evenly spaced identical rectangular cross-sectioned heat extraction inserts running parallel to the z direction. Arrows indicate the flow of heat from the heat-generating medium via the heat extraction inserts to the surrounding.

If such a set-up is large enough in the x and y directions, or insulated from the ambient, certain assumptions can be made. If each heat extraction structure is exposed to an isothermal uniform ambient in an identical way, rectangular regions drawn around each cooling structure such as those in Fig. 1 (dotted lines), would have identical temperature distributions.

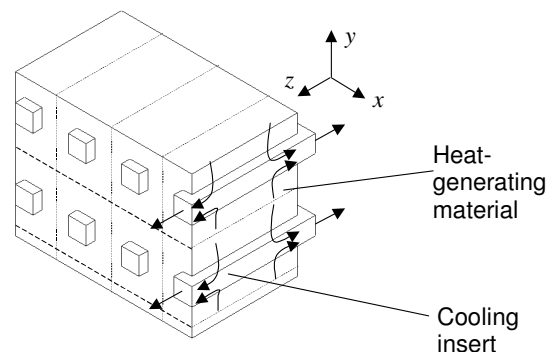


Figure 1 Cross-sectioned representation of a heat generating material with embedded cooling structures

Nomenclature

A x - y view cross-sectional area [m^2]
 a x - y view aspect ratio [dimensionless]
 $a_{C,rel}$ relative x - y view aspect ratio of cooling insert [dimensionless]
 C heat equation coefficient
 \bar{C}_G vector of heat gain coefficients
 G_M ration between volumetric heat generation and thermal conductivity [K/m^2]
 k thermal conductivity [W/mK]
 \mathbf{M} matrix of heat equation coefficients
 M_2 number of nodes in the x direction [dimensionless]
 N_2 number of nodes in the y direction [dimensionless]
 \dot{q}_C'' heat flux at exposed face of cooling insert [W/m^2]
 \dot{q}_M''' volumetric heat generation density [W/m^3]
 R thermal interface resistance [m^2K/W]
 T temperature [K]
 x Cartesian coordinate
 y Cartesian coordinate
 z Cartesian coordinate

Greek and special symbols

α fraction of volume occupied by cooling inserts [dimensionless]

γ thermal conductivity ratio [dimensionless]
 \mathcal{A} half centre-to-centre x -directional offset of neighbouring cooling inserts [m]
 a half x directional dimension of cooling insert [m]
 \mathcal{B} half centre-to-centre x directional offset of neighbouring cooling inserts [m]
 b half y directional dimension of cooling insert [m]
 Z half z directional dimension of structure [m]

Subscripts

B relative rear directional (negative z direction)
 C cooling insert
 D whole domain
 E relative easterly direction (positive x direction)
 F relative frontal direction (positive z direction)
 G heat gain or heat loss
 max maximum
 min minimum
 N relative northerly direction (positive y direction)
 S relative southerly direction (negative y direction)
 T relative current node indication
 W relative westerly direction (negative x direction)
 O reference cooling insert temperature

Furthermore due to the even spacing of the cooling structures and the equal exposure to the surroundings in both sides in the z direction, the temperature field about one such cooling structure is symmetric in all three Cartesian directions. The rectangular region around such a heat extraction structure can thus be divided into quadrants, each of which would be sufficient to represent the temperature field about such a heat extraction structure. Such a three dimensional representative quadrant domain is shown in Fig. 2 where the heat extraction insert is exposed to the surroundings on its positive z side face.

In order to obtain the steady state three-dimensional temperature distribution in such a quadrant domain, a cell-centred finite volume numerical approach was used.

The schematic representation of the grid used for this is shown in Fig. 3 . The number of nodes shown here are not necessarily the number used during simulations. An important point to note is that no nodes were defined on the interface between the cooling structure and the heat-generating medium. This is due to discontinuities that appear in solutions for cases with small or no contact resistance at the interface.

The grid used was localised uniform, which means for each block shown in Fig.3 , the grid spacing was uniform, but not necessarily uniform across the entire mesh. Uniform grid spacing was also used in the z direction.

All boundaries were defined as being adiabatic, except the positive z side face of the heat extraction insert, which had a fixed reference temperature of T_0 at $x=0$ and $y=0$, and a uniform heat flux to the surrounding. By applying the principle of conservation of energy, the steady state heat flux, \dot{q}_C'' [W/m^2], on this surface can be obtained from the dimensions of, and volumetric heat generation density, \dot{q}_M''' [W/m^3] within the representative domain:

$$\dot{q}_C'' = -\frac{\dot{q}_M''' (\mathcal{A}\mathcal{B} - ab)Z}{ab} \tag{1}$$

Here \mathcal{A} , a , \mathcal{B} , b , and Z are the dimensions of the representative domain as defined in Fig. 2 .

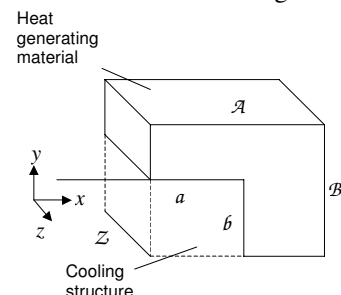


Figure 2 Schematic of the representative domain

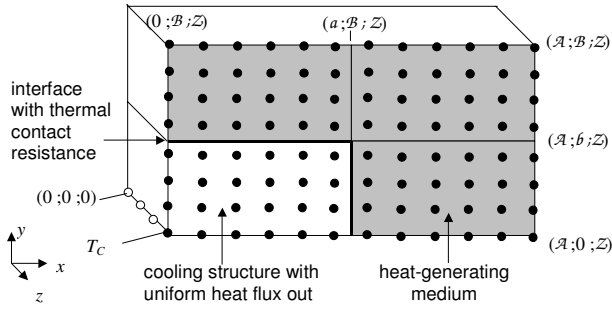


Figure 3 Meshing scheme used

Variable Definition

The aspect ratios of the overall domain and the cooling structure in the *xy*-plane were defined respectively as:

$$a_D = \frac{A}{B} \geq 1 \tag{2}$$

$$a_C = \frac{a}{b} \tag{3}$$

Only $a_D \geq 1$ were investigated, as the mirror behaviour for $a_D \leq 1$ is equivalent. For instance $a_D = 2$ would give the same results as $a_D = 0.5$ by just rotating the *x* and *y* axes by 90°.

The cross-sectional area of the entire representative domain and cooling structure in the *xy* view can be written respectively as:

$$A_D = AB \tag{4}$$

$$A_C = ab = \alpha A_D \tag{5}$$

The fraction of the entire domain volume used for heat extraction purposes are denoted by α . Five variables namely A_D [m²], a_D [dimensionless], a_C [dimensionless], α [dimensionless], and Z [m], define the geometry of the representative domain fully. Due to geometric constraints, the cooling insert aspect ratio, a_C , has maximum and minimum allowed values namely:

$$a_{C, \min} = \alpha a_D \tag{6}$$

$$a_{C, \max} = \frac{a_D}{\alpha} \tag{7}$$

The ratio between the thermal conductivity of the cooling structure, k_C [W/mK] and thermal conductivity of heat-generating material k_M [W/mK] was defined as:

$$\gamma = \frac{k_C}{k_M} \tag{8}$$

The ration between the volumetric heat-generation and thermal conductivity of the heat-generating material [K/m²] can be written as:

$$G_M = \frac{\dot{q}_M'''}{k_M} \tag{9}$$

Numerical Method

Numerical simulation involves three separated stages namely pre-processing, processing or solution, and post-processing. Pre-processing include the definition of domain dimensions, thermal properties and conditions, mesh creation, and solution method specification. Due to the large number of anticipated simulation cases that would be needed to optimise cooling structure shapes and distribution, the conventional pre-processing stage would become very time consuming when using commercially available numerical simulation software packages. For this reason it was opted to create computer code that would automatically do the pre-processing functions and would then feed the problem information straight into a solution procedure or algorithm.

A fully implicit solution algorithm approach was followed. This approach has the advantage of being computational efficient in the case of relatively small meshing schemes, and highly predictable concerning the running time needed to solve the temperature field. It is only dependent on the number of nodes in the domain and is not influenced by the physical conditions of the domain, as would be the case if a fully explicit procedure were used.

In order to use an implicit method, it is necessary to express the temperature at a node in terms of its neighbouring temperature values by means of different coefficients [3]:

$$C_T T = C_F T_F + C_S T_S + C_W T_W + C_E T_E + C_N T_N + C_B T_B + C_G \dots \tag{10}$$

Subscripts *F*, *S*, *W*, *E*, *N*, and *B* refer to the six reference directions namely “front”, “south”, “west”, “east”, “north”, and “back” respectively. Subscript *T* refer to temperature node under consideration, and *G* indicates the heat gain or heat loss of the particular node.

If there is *N* number of nodes, this will result in *N* number of equations. It is possible to express this system of equations as:

$$\mathbf{M}\bar{T} = \bar{C}_G \tag{11}$$

Here **M** is a *N*-by-*N* coefficient matrix, \bar{C}_G is a vector containing the heat gain or loss coefficient for each node, and \bar{T} is a vector containing the temperature values of all the nodes in the domain.

In order to construct such a matrix it is necessary to decide before hand on a numbering scheme for the nodes such that each node has a unique address. For a structured numbering scheme (shown in Fig. 4 for a 3x3x3 mesh) where there are M_2 number of nodes in the x direction and N_2 number of nodes in the y direction, \mathbf{M} has a banded structure as shown in Fig. 5 with seven diagonals that contain non-zero entries. Each of these diagonals contains the relevant coefficients defined in Eq. (10).

The coefficient matrix is thus a very sparsely populated matrix with the majority of entries being zero. The conventional classic method of solving the temperature vector would be to use Gauss-Jordan elimination to obtain the inverse of the matrix, but due to the high density of zero-entries there are more efficient ways of solving the temperature vector.

One such a method is LU-decomposition of the coefficient matrix into an upper and lower triangular matrix. From this back- and forward-substitution can be used to obtain the temperature solution. Due to the banded structure of \mathbf{M} , the traditional LU-decomposition algorithm can be adjusted to reduce the number of computations needed. This is done by only applying the decomposition algorithm within the band of \mathbf{M} ranging from diagonals B to F . This is a valid adjustment as the entries of lower and upper triangular matrices corresponding to the regions outside this band only contain zero entries anyway.

The number of computations needed can further be reduced if the bandwidth of \mathbf{M} is decreased. This can be done by using a different numbering scheme for the nodes in the domain according to the reverse Cuthill-McKee algorithm.

Refer to Fig. 6 for the percentage reduction in the bandwidth (compared with the structured numbering scheme) for three different size matrices at different number of nodes in the z direction after this algorithm was applied. It was found that for a structured two-dimensional mesh, where there is only one node in the z direction, there is no reduction in the bandwidth of the matrix. It is the most advantageous to apply the reverse Cuthill-McKee algorithm where the mesh has a width of two nodal point in the z direction. In the current study 10 nodes were used in the z direction. Using more than 10 nodes in the z direction, resulted in differences of less than 0.1% in solved temperature distributions.

Numerical Results

By running a sequence of simulations, the optimum cooling structure shape can be found for a particular representative domain geometry and thermal condition.

It was found that for $a_D \geq 1$, the lowest peak temperature is always associated with a cooling structure aspect ratio, a_C , in the range of $[a_D; a_{C,max}]$. A convenient way of normalising a_C is by defining a new relative cooling aspect ratio, $a_{C,rel}$:

$$a_{C,rel} = \frac{a_c - a_D}{a_{C,max} - a_D} \tag{12}$$

When $a_{C,rel} = 1$, it means that the cooling insert is at its maximum aspect ratio as shown in Fig. 7, while when $a_{C,rel} = 0$ the cooling insert has the same aspect ratio as the representative domain.

It was found that the maximum temperature in the domain, T_{max} , is directly proportional to G_M and that an increase or decrease in the cooling structure temperature, T_C , is translated directly into an identical increase or decrease in T_{max} . Mathematically this can be expressed as:

$$T_{max} - T_C \propto G_M \tag{13}$$

This means that neither G_M nor T_C has any influence on the shape of the optimum cooling geometry.

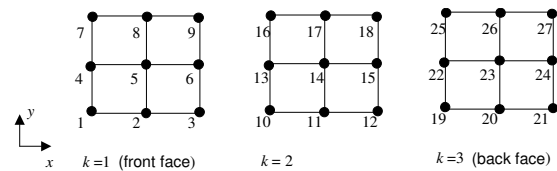


Figure 4 Structured numbering scheme used

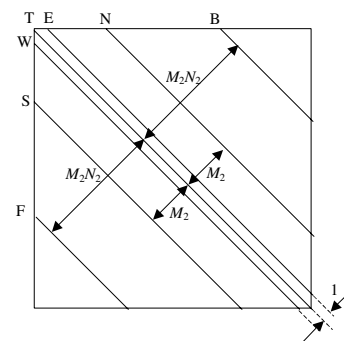


Figure 5 Banded structure of the coefficient matrix

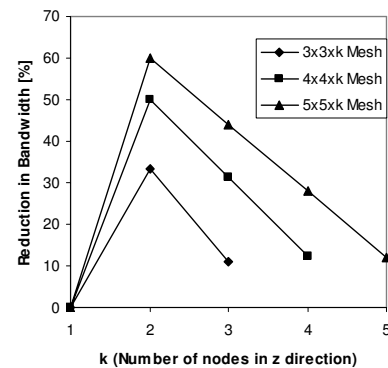


Figure 6 Reduction in matrix bandwidth after applying the Reverse Cuthill-McKee algorithm

Optimisation Results for $a_D = 1$

A domain with a square cross-sectional area is applicable to an arrangement where the cooling structure spacing in both Cartesian directions is identical.

Fig. 8 shows that for the case where there is no thermal contact resistance, the physical size of the cooling insert has little influence on its optimum shape. Similarly, in Fig. 9, the same is shown to be true of the influence of the depth of the domain.

For cases where less than approximately 70% of the domain is occupied by cooling, the optimum cooling insert shape is found to be a flat continuous “plate” as shown in Fig. 7.

Also, it was found for cases with no thermal interface resistance, that the actual values of the thermal conductivities did not play any role, but rather that the ratio between the thermal conductivities, γ , was of concern. In Fig. 10 the optimum cooling shapes for various ratios, where no thermal contact resistance is present, is given.

When however thermal contact resistance, R [m^2K/W] is introduced, it is found that none of the above mentioned trends are valid. From Figs. 11-13 it is shown that the presence of contact resistance results in the relative optimum aspect ratio deviating from the $a_{C,rel} = 1$ line at an earlier α value than in the case without the presence of contact resistance. This means that the optimum cooling shape for larger cooling fraction is no longer that of a flat continuous plate. Also as is shown in Fig. 14, that the physical sizes of the thermal conductivities influence the optimum cooling aspect ratio when interface thermal resistance is present.

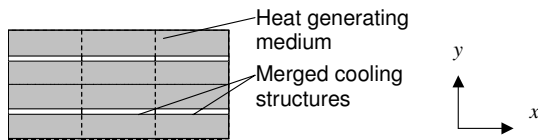


Figure 7 Physical meaning for the case where a_C is at its maximum

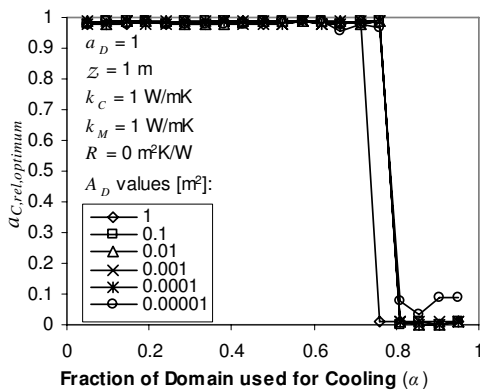


Figure 8 The influence of the physical size of the cooling structures on the optimum cooling insert shape for a mesh thickness of 1 m.

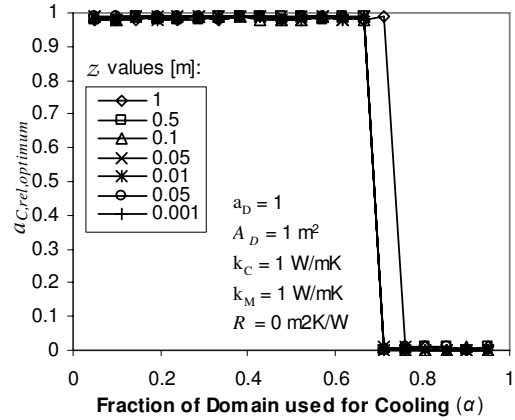


Figure 9 The influence of the z direction depth on the optimum cooling insert shape for a domain area of $1 m^2$.

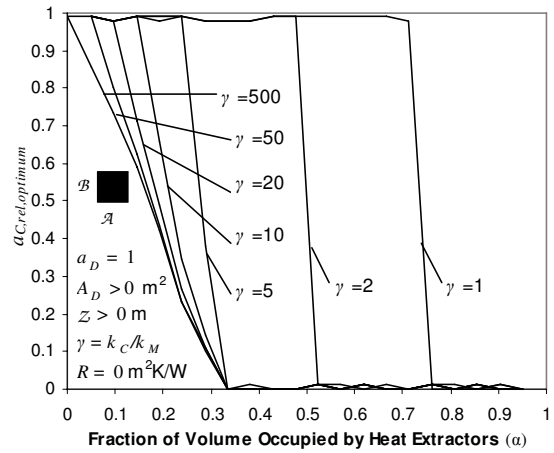


Figure 10 Influence of γ on $a_{C,rel, optimum}$ for $A_D = 1 m^2$, $Z = 0.001 m$, and $R = 0 m^2K/W$

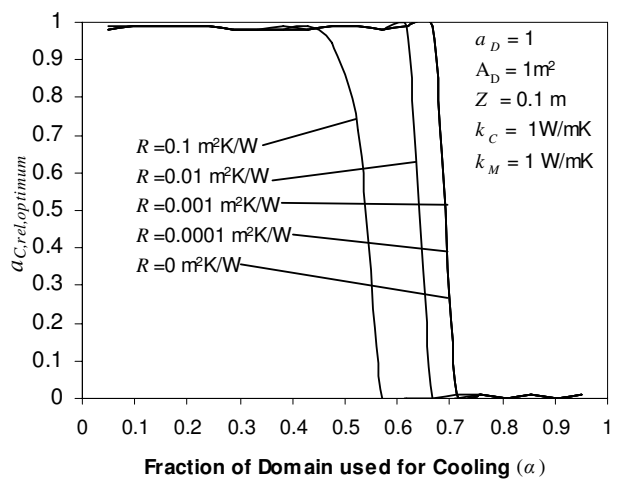


Figure 11 Influence of thermal contact resistance on the optimum cooling shape for $A_D = 1 m^2$ and $Z = 0.1 m$

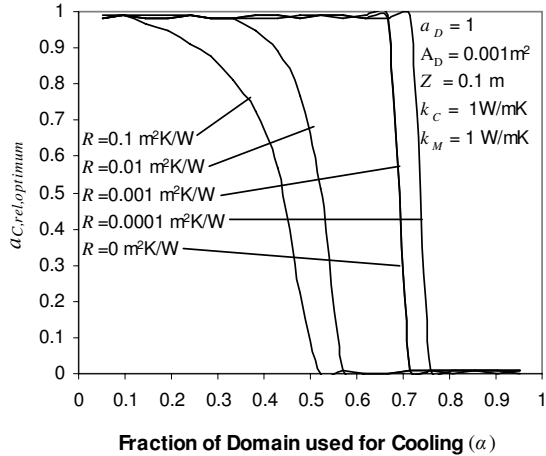


Figure 12 Influence of thermal contact resistance on the optimum cooling shape for $A_D = 0.001 \text{ m}^2$ and $Z = 0.1 \text{ m}$

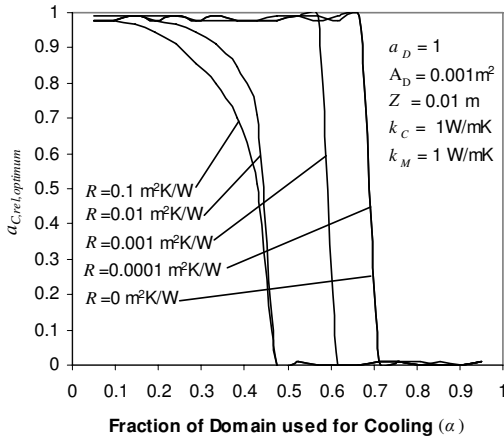


Figure 13 Influence of thermal contact resistance on the optimum cooling shape for $A_D = 0.001 \text{ m}^2$ and $Z = 0.01 \text{ m}$

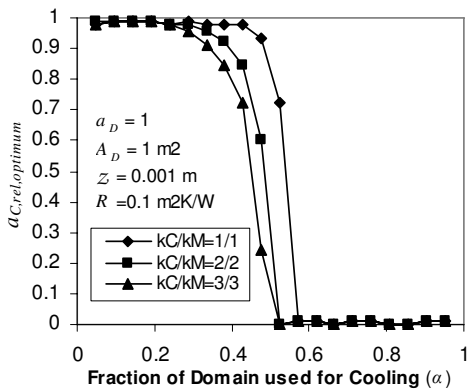


Figure 14 Non-zero R for a constant ratio of thermal conductivity for $A_D = 1 \text{ m}^2$ and $Z = 0.001 \text{ m}$

Optimisation Results for $a_D = 2$

A domain with an aspect ratio of 2 represents a situation where the centre-to-centre distance between two adjacent cooling structures in one Cartesian coordinate direction is twice the centre-to-centre distance of two neighbouring cooling structures in the other Cartesian direction.

Fig. 15 gives the behaviour of the optimum cooling shape for $a_D = 2$ at various R -values. It was found that as before the presence of thermal contact resistance influences the optimum shape. It was also found that unlike $a_D = 1$, the optimum cooling shape never has the same aspect ratio as the representative domain. It has a higher tendency to have a flat plate geometry as an optimum cooling shape.

For smaller cooling structures it was found that the optimum geometry graphs fan out a bit as indicated in Fig. 16 for different R values. The influence of the conductivity ratio was found to be small.

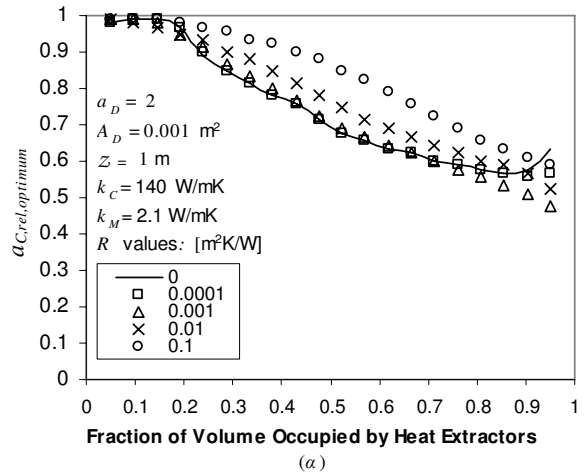


Figure 15 Influence of R on the optimum cooling shape for $a_D = 2$.

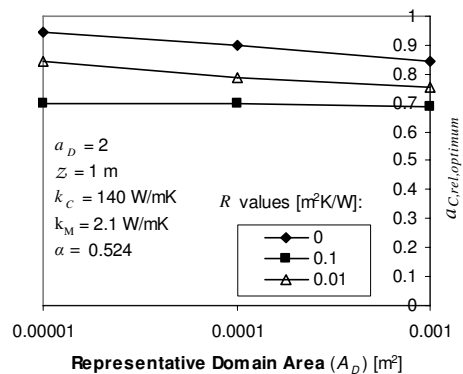


Figure 16 Influence of A_D for $a_D = 2$ at $\alpha = 0.524$

Optimisation Results for $a_D = 5$

As was found for $a_D = 2$, the case where $a_D = 5$, has an even higher tendency toward optimum cooling shapes of a flat plate. From Fig. 17 it can also be seen that the influence of the thermal contact resistance is also not as severe as before. Similarly the physical size of the cooling structure, A_D , has a lesser influence.

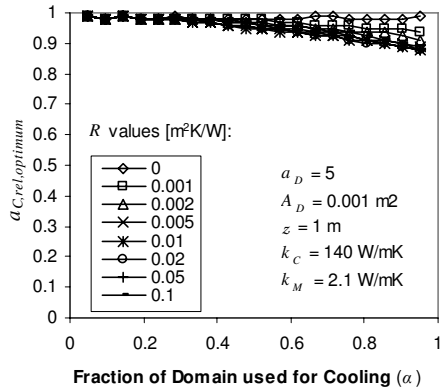


Figure 17 Optimum cooling shape aspect ratios for $a_D = 5$ and various R values.

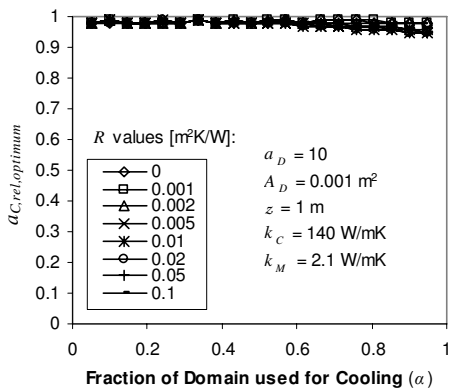


Figure 18 Optimum cooling shape aspect ratios for $a_D = 10$ and various R values.

Optimisation Results for $a_D = 10$

A similar trend is found to be true for higher representative domain aspect ratios as is shown in Fig. 18. In this case it was observed that almost through the entire spectrum of domain fractions used by cooling the optimum cross-sectional shape was that of a flat plate.

Dimensional Scaling

It is also important to determine when it is advantageous to optimise the cross sectional aspect ratio of the extractor inserts in order to accommodate higher heat generation densities while maintaining a certain maximum temperature within the representative

domain. Fig. 19 shows, for a case with no internal interface thermal resistance, that the effectiveness of the heat extractor becomes less dependent on its cross sectional shape as the ratios of A_D to Z^2 decreases. For low ratios of A_D to Z^2 , where the domain of a single insert becomes increasingly slender, the advantage of optimising the cross section in order to support higher heat-generation levels diminishes.

The advantage of inserting heat extractors however does not diminish, but rather the effectiveness thereof for slender domains are more dependent on the fraction of the total volume occupied by the heat extraction system α , rather than the cross sectional shape thereof. It would thus be sensible in such cases to use a cross-sectional geometry that is easier to manufacture or a geometry that would conform to possible other restrictions. Similar trends were obtained for beryllium oxide and synthetic diamond inserts. However, for the case where thermal contact resistance is present it was found that unlike the trend shown in Fig. 19, the influence of the cross-sectional shape remains present for low A_D to Z^2 ratios.

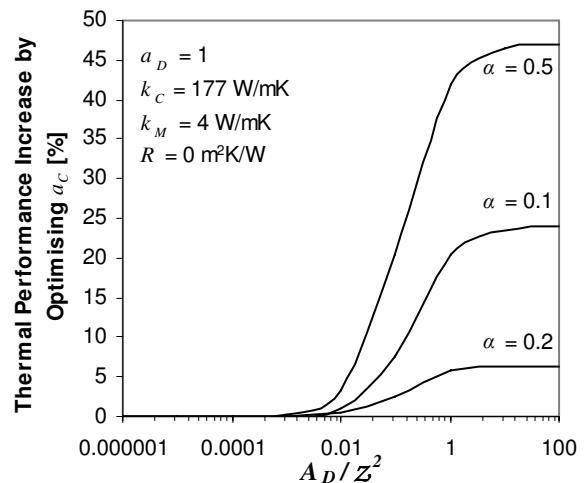


Figure 19 Additional allowable increase in heat generation density after geometric optimisation

Conclusions

It was found that there are 7 variables that determine what the optimum embedded cooling insert cross-sectional aspect ratio will be, namely a_D , A_D , α , Z , R , k_M , and k_C . When no thermal contact resistance is presents it seems as if this list can be reduced to a_D , α , and γ .

The actual temperature values within the heat-generating medium will however be dependent on all the above given parameters as well as the reference cooling temperature, T_0 and the volumetric heat generation, \dot{q}_M . The exact influence of the thermal contact resistance is difficult to describe from the presently available data, and more investigation will be needed in this regard.

Indications are that as the domain aspect ratio is increased, the tendency for the optimum cooling structure to be a continuous flat plate increases.

References

- [1] Van Wyk J.D., Strydom J.T., Zhao L., Chen R., Review of the development of high density integrated technology for electromagnetic power passives, Proceedings of the 2nd International Conference on Integrated Power Systems (CIPS), 2002, pp. 25-34
- [2] Barbosa P., Lee F.C., Van Wyk J.D., Boroyevich D., Scott E., Thole K., Odendaal H., Liang Z., Pang Y., Sewell E., Chen J., and Yang B., An overview of IPEM-based modular implementation for distributed power systems, Center for Power Electronics Systems (CPES) Power Electronics Seminar, Virginia Tech, 674 Whittemore Hall, Campus Mail Code 0179, Blacksburg, VA 24061, 2002, pp 70-76
- [3] Patankar S.V., Numerical heat transfer and fluid flow, Hemisphere (Washington D.C.) , 1980